Research Article Vol. 8, No. 8 / August 2020 / Photonics Research 1375

PHOTONICS Research

High-gain amplification for femtosecond optical vortex with mode-control regenerative cavity

Shuiqin Zheng,[1,2,3] Zhenkuan Chen,[1,3] Qinggang Lin,[1] Yi Cai,[1] Xiaowei Lu,[1] Yanxia Gao,[1,4] Shixiang Xu,[1,*] and Dianyuan Fan[3]

[1]Shenzhen Key Laboratory of Micro-Nano Photonic Information Technology, College of Physics and Optoelectronics Engineering, Shenzhen University, Shenzhen 518060, China
[2]Photonics Laboratory, Division of Computer, Electrical, and Mathematical Sciences and Engineering, King Abdullah University of Science and Technology (KAUST), Thuwal 23955-6900, Saudi Arabia
[3]SZU-NUS Collaborative Innovation Center for Optoelectronic Science & Technology, Key Laboratory of Optoelectronic Devices and Systems of Ministry of Education and Guangdong Province, Shenzhen University, Shenzhen 518060, China
[4]e-mail: gyx@szu.edu.cn
*Corresponding author: shxxu@szu.edu.cn

Received 24 February 2020; revised 21 May 2020; accepted 19 June 2020; posted 22 June 2020 (Doc. ID 390963); published 24 July 2020

Ultra-intense femtosecond vortex pulses can provide an opportunity to investigate the new phenomena with orbital angular momentum (OAM) involved in extreme cases. This paper reports a high gain optical vortex amplifier for intense femtosecond vortex pulses generation. Traditional regeneration amplifiers can offer high gain for Gaussian mode pulses but cannot amplify optical vortex pulses while maintaining the phase singularity because of mode competition. Here, we present a regeneration amplifier with a ring-shaped pump. By controlling the radius of the pump, the system can realize the motivation of the Laguerre–Gaussian [$LG_{0,1(-1)}$] mode and the suppression of the Gaussian mode. Without seeds, the amplifier has a donut-shaped output containing two opposite OAM states simultaneously, as our prediction by simulation. If seeded by a pulse of a topologic charge of 1 or −1, the system will output an amplified $LG_{0,1(-1)}$ mode pulse with the same topologic charge as the seed. To our knowledge, this amplifier can offer the highest gain as 1.45×10^6 for optical vortex amplification. Finally, we obtain a 1.8 mJ, 51 fs compressed optical vortex seeded from a 2 nJ optical vortex.

https://doi.org/10.1364/PRJ.390963

1. INTRODUCTION

An optical vortex beam is a structured beam with a spiral phase $e^{-il\phi}$ in the azimuthal direction ϕ perpendicular to the propagation direction [1–3]. These beams carrying an orbital angular momentum (OAM) of $l\hbar$ per photon have opened a route to many promising applications, such as optical communication [4–8], laser ablation [9–12], and micromanipulation [13–15]. These applications can benefit from technologies of optical vortex generation, which can be divided into external modulation outside the cavity [16–20] and direct generation within the cavity [21–23]. Direct generation may face multi-mode superposition, which can be divided into coherent superposition and incoherent superposition [24,25]. With the increase of the peak power of the optical vortex, novel phenomena are emerging. The ultra-intense, ultra-short optical vortex pulse can provide an opportunity to investigate the new phenomena with OAM involved in extreme cases [26–29]. The spiral phase can be introduced to the ultra-short Gaussian mode laser by external modulation through a spiral phase plate [19,28], fork grating [30–34], and spatial light modulator [11,35]. Unfortunately, such methods for ultra-intense cases pose a significant challenge, owing to technical difficulties like optical element damage and the dispersion hindering the synthesis of a high-power broadband optical vortex. As the other way for generation of ultra-short vortices, the direct generation from the mode-locked laser was proved [36,37]. However, this way also cannot generate ultra-short vortices with ultra-high intensity.

Looking back to the development history of ultra-short lasers, we can see that amplification technology plays a very important role in the generation of ultra-short pulses with ultra-high intensity [38,39]. Regenerative amplification can provide a large gain [40], and chirped pulse amplification (CPA) can help to reduce the damage and nonlinear effects [41]. The Ti:sapphire (Ti:S)-based amplifier plays an important role in delivering high peak power [42]. For the ultra-intense, ultra-short optical vortex generation, the blessing of amplification technologies may be indispensable. Compared with conventional ultra-short pulse amplifiers, the input and output of an optical vortex amplifier (OVA) should be both optical vortices with the same topologic charge, and some efforts have been made. A single pass of two Nd-doped yttrium aluminum garnet (Nd:YAG) rods can amplify the optic vortex to several times [43]. A multi-pass amplifier for femtosecond optical vortex pulses in a CPA system with a gain level of 10 was demonstrated [30]. Optical parametric amplification for ultrashort optical vortex pulses generation makes a gain level up to 10^2 [44–46]. As far as we know, currently, there are no OVAs that can reach a gain level of 10^6, because these amplifiers cannot make the vortex beam pass through the gain medium for enough times.

In this paper, we develop a high-gain OVA whose gain reaches the 10^6 level based on regenerative amplification. First, we show that the conventional regenerative amplifier (RA) could not amplify the optical vortex, and the vortex seed will degenerate to a Gaussian beam because of mode competition. Then, to overcome this problem, we pump the RA with the ring-shaped laser for controlling mode competition. Our simulations show that choosing the right pump radius can suppress Gaussian mode generation and increase the gain of the target Laguerre–Gaussian (LG) mode. Therefore, one LG mode can be amplified from a weak vortex seed while maintaining the topological charge (TC) and the spiral phase. Finally, an OVA for the $LG_{0,1(-1)}$ mode has been built experimentally with an amplification gain of up to 1.45×10^6 for a 2 nJ vortex seed. Based on the OVA, the 51 fs, 1.8 mJ compressed optical vortex has been obtained.

2. MODE COMPETITION IN A REGENERATIVE AMPLIFIER

Regenerative amplification has the highest gain among all amplification technologies because the pulse can pass through the gain medium for enough times. It is well known that an RA is an active laser cavity that works as a Q-switched laser operating at the cavity dumping mode with a weak seed instead of oscillation from noise. $LG_{p,l}$ modes are the self-consistent modes of a cylindrically symmetrical cavity, where p is the index of the radial order, and l is the TC. The fundamental mode is the $LG_{0,0}$, which is also named the Gaussian mode. The seed of the RA should be matched to the most competitive self-consistent mode (usually a Gaussian mode) of the cavity for effective amplification. Traditionally, a Gaussian mode seed is injected into the cavity, and we can obtain an amplified Gaussian output. In spite of the occurrence of mode mismatching, the seed can be still amplified, but it is pulled towards the Gaussian mode. As shown in Fig. 1, a 2 nJ vortex pulse with $l = 1$ evolves into a Gaussian mode during amplification. Unfortunately, the Gaussian mode does not carry any OAM, which means that we cannot amplify vortex pulses

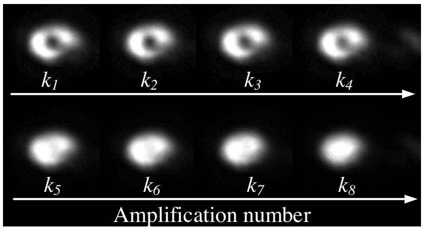

Fig. 1. Evolution of an optical vortex seed with $l = 1$ in a conventional RA and the amplification number $k_n = 4n - 3$.

directly with a conventional RA. Obviously, the reason for this is the mode competition.

In order to overcome the mode competition and realize the amplification of vortex pulses, we need the net gain of the target LG mode carrying target OAM greater than that of other modes, particularly the Gaussian mode. This is also the key to the vortex emission within the cavity, and some methods have been reported, such as a spot-defect mirror [47] and a ring-shaped pump [36,48,49]. Here, we choose the ring-shaped pump for the suppression of the Gaussian mode and excitation of the vortex modes. Our setup is reformed from a commercial 1 kHz 800 nm Ti:S RA (Coherence Inc., Legend-Elite-He). This RA without a beam expander (BE) and convex axicon (CA) is optimized in the Gaussian mode, and all components do not have further adjustment after the optimization except for the pump-related components. As shown in Fig. 2, the ring-shaped pump is realized by using a CA (Thorlabs, AX2505-A) to modulate a 50 ns, 15 mJ, 532 nm beam [50]. Besides, a variable BE is required to adjust the pump radius (the pump radius is inversely proportional to the beam expansion ratio), and the expansion ratio is set at 3.5 for the motivating of the $LG_{0,1(-1)}$ mode.

For an active cavity without seed, its initial signal starts from the noise, and the final output mode is determined by the gains of modes. The differences in these gains can be reflected in the mode probabilities of the output. For our RA, the concerned LG modes in the output mainly include $LG_{0,0}$, $LG_{0,1}$, and $LG_{0,-1}$. The purity $\rho_{p,l}$ of $LG_{p,l}$ in the optical field E for a coherent superposition can be expressed as

$$\rho_{p,l} = \frac{\langle E|LG_{p,l}\rangle\langle LG_{p,l}|E\rangle}{\langle E|E\rangle\langle LG_{p,l}|LG_{p,l}\rangle}, \quad (1)$$

where the inner product $\langle B|A\rangle$ of two fields A and B is defined as $\iint B^*(x,y)A(x,y)\mathrm{d}x\mathrm{d}y$. We simulate the laser oscillation from noise with the different radii of the ring-shaped pump or different expansion ratios of BE using the method proposed in Ref. [51]. First, we set the expansion ratio of BE as four. Our simulations start with different noises each time, and we can obtain the different outputs oscillating from the different noises. For an output, we can get the corresponding purities of $LG_{0,1}$, $LG_{0,-1}$, and $LG_{0,0}$ as $(\rho_{0,1}, \rho_{0,-1}, \rho_{0,0})$. We simulate

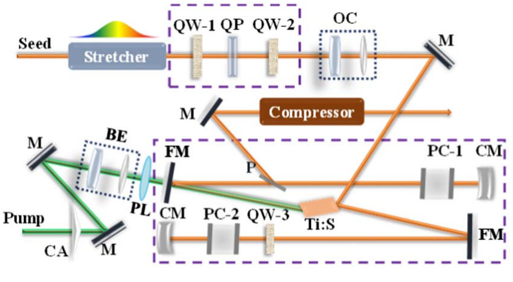

Fig. 2. Setup of the proposed RA. QW, quarter-wave plate; QP, Q-plate; OC, optical coupling system; M, plane mirror; CM, concave mirror, $R = -1$ m; PM, fold mirror, $R = 0.9$ m; PC, Pock cell; BE, beam expander; P, polarizer; PL, pump lens, $f = 30$ cm; CA, convex axicon, base angle of 0.5°; Ti:S, Ti:sapphire, length of 25.4 mm.

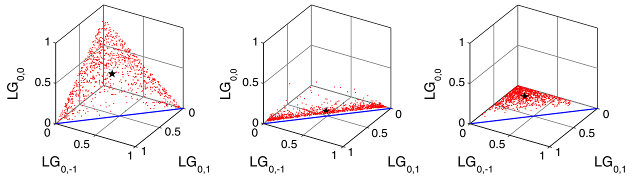

Fig. 3. Simulations of laser oscillations from noises with the different ring-shaped pump radii. Expansion ratios are (a) 4, (b) 3.5, and (c) 3.

1000 oscillations from different noises, and the purities of the 1000 outputs are obtained. As shown in Fig. 3(a), the $(\rho_{0,1}, \rho_{0,-1}, \rho_{0,0})$ are plotted in a three-dimensional coordinate, while the black star is for the average mode purities or mode probabilities $(\bar{\rho}_{0,1}, \bar{\rho}_{0,-1}, \bar{\rho}_{0,0})$. As can be seen from Fig. 3(a), $LG_{0,1}$ and $LG_{0,-1}$ start to appear, but $LG_{0,0}$ is not well suppressed. When the expansion ratio is set as three, $LG_{0,0}$ is well suppressed ($\rho_{0,0} \to 0$), as shown in Fig. 3(c). However, $LG_{0,1}$ and $LG_{0,-1}$ are not very well motivated because the pump radius is too large. However, if the expansion ratio is 3.5, $LG_{0,1}$ and $LG_{0,-1}$ are well motivated, while $LG_{0,0}$ is well suppressed, as shown in Fig. 3(b). The purities lay near the blue line, which represents $\rho_{0,1} + \rho_{0,-1} = 1$, and the mode probabilities are near the center of the blue line. Because the ring-shaped pump is not selective between $LG_{0,1}$ and $LG_{0,-1}$, the gains for these modes are the same, and we cannot select a unique vortex mode from the series of self-consistent LG modes by the ring-shaped pumped cavity. Consequently, the system generates the two modes with the same possibility in the absence of external seeds.

For the RA, the final output depends on not only the gain of each mode, but also the mode and energy of the input seed. We simulate the RA seeding with a vortex pulse with $l = 1$. For different seed energies, our simulation also runs 1000 times, and the mode probabilities are obtained. As shown in Fig. 4, if the seed is weak enough, $LG_{0,1}$ and $LG_{0,-1}$ are the two most possible modes to survive with the same possibility of 45%. At the same time, the $LG_{0,0}$ mode is well suppressed. The $LG_{0,1}$ mode purity increases with the increase of seed energy, while $LG_{0,-1}$ mode purity decreases. If the seed energy rises to 0.01 nJ, the purity goes up to 96% for $LG_{0,1}$ but drops to 0.8% for $LG_{0,-1}$, while $LG_{0,0}$ always keeps its purity less than 0.12%. Our simulations also find that, if the TC of the seed changes to −1 instead of 1, the high probability mode will change to $LG_{0,-1}$ instead of $LG_{0,1}$.

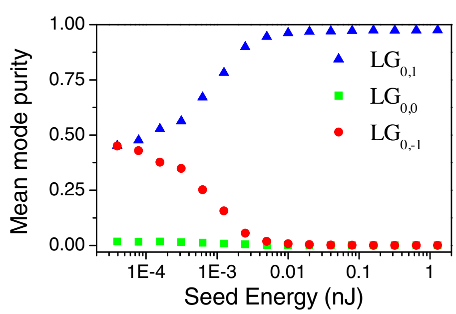

Fig. 4. Simulation of vortex amplification with different seed energies.

3. EXPERIMENTAL RESULTS AND DISCUSSIONS

In our experiments, we first align BE for matching the radius of the ring-shaped pump for the motivation of $LG_{0,1(-1)}$ and the suppression of $LG_{0,0}$. The expansion ratio of BE is chosen as 3.5 according to our simulation. Figure 5(a) shows the ring-shaped pump at one of the Ti:S surfaces. Correspondingly, the output beam profile from the RA without seeding is shown in Fig. 5(b). The donut-shaped distribution of the output implies that $LG_{0,0}$ has been successfully suppressed. The Dammann vortex grating can be used to check the TC of the output by measuring whether the pattern on the corresponding diffraction order is solid [52]. Figure 5(c) is the phase structure of our Dammann vortex grating, which is loaded into a spatial light modulator. Figure 5(d) shows the simulated far-field diffraction patterns with parallel illumination. By determining whether the spots on the green box are solid, we can find out whether the beam contains an OAM component with $l = 0$, while the blue and red boxes are for $l = +1$ and −1. Figure 5(e) presents the measured far-field spots after the Dammann vortex grating from the output of the unseeded RA. A very bright solid spot in the center is an exception, which is from the strong zero-order diffraction. Other solid spots only locate within the blue and red boxes, which means the output beam includes both $LG_{0,1}$ and $LG_{0,-1}$ modes.

Our vortex seed with $l = 1$ is converted from a Gaussian mode pulse from a mode-locked oscillator with a Q-plate (QP) and two achromatic quarter-wave plates (QW-1 and QW-2), as shown in Fig. 2. The final seed before the incident to the system has the pulse energy of 2 nJ, and we check the TC of the seed by a cylindrical lens [53]. Figure 6(a) is the recorded spatial profile of the seed focused by a cylindrical lens, which features one dark stripe across the beam spot, showing that the seed has a TC of one. The stripe orientation depends on whether the TC is positive or negative. Correspondingly, the amplified output is recorded as Fig. 6(b), which also presents a donut-shaped profile. The corresponding far-field distribution after the Dammann vortex grating is shown in Fig. 6(c). Compared with Fig. 5(e), its solid spots only exist inside the blue

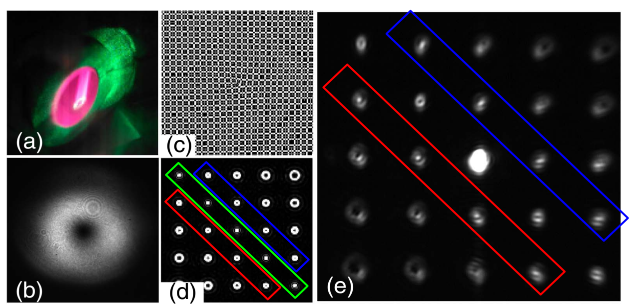

Fig. 5. (a) Ring-shaped pump on one of the Ti:S surfaces, (b) the donut-shaped output from the unseeded RA, (c) the phase structure of our Dammann vortex grating, (d) the corresponding far-field with parallel illumination, and (e) the measured far-field illuminated by the output of the unseeded RA.

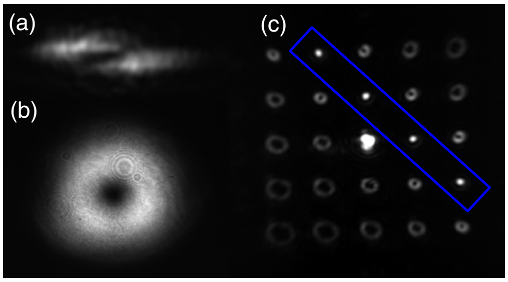

Fig. 6. Recorded spatial intensities of the seed with $l = 1$: (a) the seed focused by a cylindrical lens, (b) the output spatial intensity distribution, and (c) the far-field distribution after Dammann vortex grating.

box. This means that the output contains $LG_{0,1}$ mode only and has the same TC as the seed. Then, we rotate simultaneously QW-1 and QW-2 with an angle of 90° to change the TC value of the seed from 1 to −1. Compared with Fig. 6(a), the cylindrical lens focused pattern of the seed changed the orientation of the tilted dark stripe, as shown in Fig. 7(a). This implies that the seed changes to an opposite TC. As shown in Fig. 7(b), the amplified output seeded with $l = -1$ has a similar profile as that in Figs. 5(b) and 6(b). Compared with Fig. 6(c), Fig. 7(c) confirms further that the output has changed its TC value from +1 to −1, showing that our RA can keep the output maintaining the same TC from the seed. From Fig. 5(e), the rings around the spots are oval and disconnected on the minor axis sides. We infer that they result from the astigmatisms due to the slight misalignment of the Fourier lens after the Dammann vortex grating. The slightly oval rings on both sides of the red and blue boxes in Figs. 6(c) and 7(c) are also caused by the astigmatism.

From Fig. 6(b), we can get different cross-section intensity distributions across the center along with different directions; then, we obtain the average cross section from the orientations, as shown as the black line in Fig. 8(a). The dashed red line is the theoretical fit by $LG_{0,1}$, which agrees with the average data very well. For the amplified LG_{01} pulse, the spiral phase distribution is verified by the Dammann vortex grating, and we can determine the phase term as $e^{-il\phi}$ with $l = 1$. The amplitude term can be obtained from the captured intensity. With these two terms, the mode purity of LG_{01} from the output is 95% according to Eq. (1). This means that our RA outputs

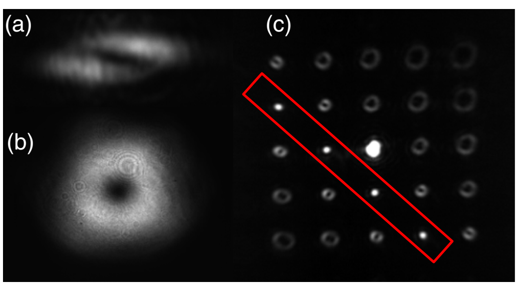

Fig. 7. Recorded spatial intensities of the seed with $l = -1$: (a) the seed focused by a cylindrical lens, (b) the output spatial intensity distribution, and (c) the far-field distribution after Dammann vortex grating.

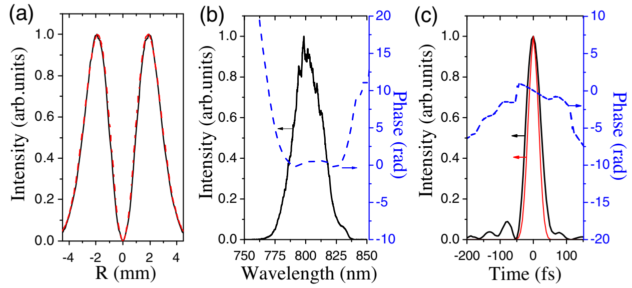

Fig. 8. (a) Spatial cross-section intensity of the amplified $LG_{0,1}$ vortex: the average from the different orientations (black line) and theoretical fitting (dashed red line); (b) the spectral intensity and phase of the amplified $LG_{0,1}$ pulse; (c) the temporal intensity and phase of the amplified $LG_{0,1}$ pulse (black and blue lines) and the temporal intensity of corresponding Fourier-transform-limited pulse (red line).

high-quality $LG_{0,1}$ pulses. Compared with the same RA cavity with the Gaussian pump, our RA with a ring-shaped pump has smaller gain under the same pump power because of the deduction of pump density. Smaller net gain will result in larger amplification pass number N for saturated output and smaller output power. According to our experiment, the N for saturated amplification is 53 for the ring-shaped pump, and it is 27 for the Gaussian pump under the same pump energy of 15 mJ. Before entering the compressor, the output pulse energies are 2.9 mJ for the ring-shaped pump and 4.5 mJ for the Gaussian pump. From this, the gain of our OVA is 1.45×10^6, and the corresponding output energies are 1.8 mJ and 3.2 mJ after compression. The pulse durations of the outputs have been measured with spectral phase interferometry for direct electric-field reconstruction (SPIDER). The spectral intensity and phase of the amplified $LG_{0,1}$ pulse are shown in Fig. 8(b). Figure 8(c) shows that the $LG_{0,1}$ pulse duration is about 51 fs with the black line, which is wider than 45.3 fs of the Gaussian pulse. This is because the larger N implies to induce larger high-order material dispersion, which cannot be compensated by a compressor. However, the red line in Fig. 8(c) reveals that the spectrum of the amplified $LG_{0,1}$ pulse can support a Fourier-transform-limited pulse with a pulse duration as short as 35 fs.

4. CONCLUSIONS

Summarily, in order to overcome the mode competition problem for the amplification of an optical vortex in RA, we develop a high-gain OVA with the mode-control cavity. The RA is pumped with the ring-shaped laser for controlling mode competition. Our simulation shows that choosing the right radius of the pump can suppress the generation of Gaussian mode and increase the gain of $LG_{0,1(-1)}$ mode. In our experiment, an RA for $LG_{0,1(-1)}$ mode is built. It verifies that, without a seeding, the amplifier has a donut-shaped output containing two opposite OAM states simultaneously. By seeding pulses with the topologic charge of one, the system will output amplified $LG_{0,1}$ mode pulses with the same topologic charge as the seed. The sign of the output TC can be changed accordingly by changing that of the vortex seed. This shows that our OVA, whose gain is 1.45×10^6 for 2 nJ seed, can maintain the TC and the spiral phase of the vortex seed during amplification. Finally, a 1.8 mJ, 51 fs optical vortex after compression is obtained.

Funding. National Natural Science Foundation of China (61490710, 61705132, 61775142); Shenzhen Basic Research Project on Subject Layout (JCYJ20170412105812811); Shenzhen Basic Research Projects (JCYJ20190808115601653, JCYJ20190808164007485).

Disclosures. The authors declare no conflicts of interest.

REFERENCES

1. A. M. Yao and M. J. Padgett, "Orbital angular momentum: origins, behavior and applications," Adv. Opt. Photon. **3**, 161–204 (2011).
2. L. Allen, M. W. Beijersbergen, R. J. C. Spreeuw, and J. P. Woerdman, "Orbital angular momentum of light and the transformation of Laguerre–Gaussian laser modes," Phys. Rev. A **45**, 8185–8189 (1992).
3. S. Franke-Arnold, L. Allen, and M. Padgett, "Advances in optical angular momentum," Laser Photon. Rev. **2**, 299–313 (2008).
4. A. E. Willner, H. Huang, Y. Yan, Y. Ren, N. Ahmed, G. Xie, C. Bao, L. Li, Y. Cao, Z. Zhao, J. Wang, M. P. J. Lavery, M. Tur, S. Ramachandran, A. F. Molisch, N. Ashrafi, and S. Ashrafi, "Optical communications using orbital angular momentum beams," Adv. Opt. Photon. **7**, 66–106 (2015).
5. J. Wang, J. Yang, I. M. Fazal, N. Ahmed, Y. Yan, B. Shamee, A. E. Willner, K. Birnbaum, J. Choi, B. Erkmen, S. Dolinar, and M. Tur, "25.6-bit/s/Hz spectral efficiency using 16-QAM signals over pol-muxed multiple orbital-angular-momentum modes," in *IEEE Photonic Society 24th Annual Meeting* (2011), Vol. **58**, pp. 587–588.
6. T. Lei, M. Zhang, Y. Li, P. Jia, G. N. Liu, X. Xu, Z. Li, C. Min, J. Lin, C. Yu, H. Niu, and X. Yuan, "Massive individual orbital angular momentum channels for multiplexing enabled by Dammann gratings," Light Sci. Appl. **4**, e257 (2015).
7. J. Wang, "Advances in communications using optical vortices," Photon. Res. **4**, B14–B28 (2016).
8. E. Stegenburgs, A. Bertoncini, A. Trichili, M. S. Alias, T. K. Ng, M. Alouini, C. Liberale, and B. S. Ooi, "Near-infrared OAM communication using 3D-printed microscale spiral phase plates," IEEE Commun. Mag. **57**, 65–69 (2019).
9. J. Hamazaki, R. Morita, K. Chujo, Y. Kobayashi, S. Tanda, and T. Omatsu, "Optical-vortex laser ablation," Opt. Express **18**, 2144–2151 (2010).
10. T. Omatsu, K. Chujo, K. Miyamoto, M. Okida, K. Nakamura, N. Aoki, and R. Morita, "Metal microneedle fabrication using twisted light with spin," Opt. Express **18**, 17967–17973 (2010).
11. B. Wetzel, C. Xie, P. Lacourt, J. M. Dudley, and F. Courvoisier, "Femtosecond laser fabrication of micro and nano-disks in single layer graphene using vortex Bessel beams," Appl. Phys. Lett. **103**, 241111 (2013).
12. F. Courvoisier, R. Stoian, and A. Couairon, "Ultrafast laser micro- and nano-processing with nondiffracting and curved beams," Opt. Laser Technol. **80**, 125–137 (2016).
13. S. R. Lee, J. Kim, S. Lee, Y. Jung, J. K. Kim, and K. Oh, "All-silica fiber Bessel-like beam generator and its applications in longitudinal optical trapping and transport of multiple dielectric particles," Opt. Express **18**, 25299–25305 (2010).
14. C. Liu, Z. Guo, Y. Li, X. Wang, and S. Qu, "Manipulating ellipsoidal micro-particles by femtosecond vortex tweezers," J. Opt. **17**, 035402 (2015).
15. N. Eckerskorn, R. Bowman, R. A. Kirian, S. Awel, M. Wiedorn, J. Küpper, M. J. Padgett, H. N. Chapman, and A. V. Rode, "Optically induced forces imposed in an optical funnel on a stream of particles in air or vacuum," Phys. Rev. Appl. **4**, 064001 (2015).
16. P. Chen, B. Wei, W. Ji, S. Ge, W. Hu, F. Xu, V. Chigrinov, and Y. Lu, "Arbitrary and reconfigurable optical vortex generation: a high-efficiency technique using director-varying liquid crystal fork gratings," Photon. Res. **3**, 133–139 (2015).
17. J. Xin, K. Dai, L. Zhong, Q. Na, and C. Gao, "Generation of optical vortices by using spiral phase plates made of polarization dependent devices," Opt. Lett. **39**, 1984–1987 (2014).
18. Y. Tokizane, K. Oka, and R. Morita, "Supercontinuum optical vortex pulse generation without spatial or topological-charge dispersion," Opt. Express **17**, 14517–14525 (2009).
19. N. Matsumoto, T. Ando, T. Inoue, Y. Ohtake, N. Fukuchi, and T. Hara, "Generation of high-quality higher-order Laguerre–Gaussian beams using liquid-crystal-on-silicon spatial light modulators," J. Opt. Soc. Am. A **25**, 1642–1651 (2008).
20. K. J. Moh, X. C. Yuan, D. Y. Tang, W. C. Cheong, L. S. Zhang, D. K. Y. Low, X. Peng, H. B. Niu, and Z. Y. Lin, "Generation of femtosecond optical vortices using a single refractive optical element," Appl. Phys. Lett. **88**, 091103 (2006).
21. M. Okida, T. Omatsu, M. Itoh, and T. Yatagai, "Direct generation of high power Laguerre–Gaussian output from a diode-pumped Nd:YVO_4 1.3-μm bounce laser," Opt. Express **15**, 7616–7622 (2007).
22. D. J. Kim and J. W. Kim, "Direct generation of an optical vortex beam in a single-frequency Nd:YVO_4 laser," Opt. Lett. **40**, 399–402 (2015).
23. Y. Zhao, Z. Wang, H. Yu, S. Zhuang, H. Zhang, X. Xu, J. Xu, X. Xu, and J. Wang, "Direct generation of optical vortex pulses," Appl. Phys. Lett. **101**, 031113 (2012).
24. I. A. Litvin, S. Ngcobo, D. Naidoo, K. Ait-Ameur, and A. Forbes, "Doughnut laser beam as an incoherent superposition of two petal beams," Opt. Lett. **39**, 704–707 (2014).
25. D. Naidoo, K. Aït-Ameur, M. Brunel, and A. Forbes, "Intra-cavity generation of superpositions of Laguerre–Gaussian beams," Appl. Phys. B **106**, 683–690 (2012).
26. D. Pengel, S. Kerbstadt, D. Johannmeyer, L. Englert, T. Bayer, and M. Wollenhaupt, "Electron vortices in femtosecond multiphoton ionization," Phys. Rev. Lett. **118**, 053003 (2017).
27. A. Leblanc, A. Denoeud, L. Chopineau, G. Mennerat, P. Martin, and F. Quéré, "Plasma holograms for ultrahigh-intensity optics," Nat. Phys. **13**, 440–443 (2017).
28. D. Gauthier, P. R. Ribič, G. Adhikary, A. Camper, C. Chappuis, R. Cucini, L. F. DiMauro, G. Dovillaire, F. Frassetto, R. Géneaux, P. Miotti, L. Poletto, B. Ressel, C. Spezzani, M. Stupar, T. Ruchon, and G. De Ninno, "Tunable orbital angular momentum in high-harmonic generation," Nat. Commun. **8**, 14971 (2017).
29. L. Rego, K. M. Dorney, N. J. Brooks, Q. L. Nguyen, C. Liao, J. San Román, D. E. Couch, A. Liu, E. Pisanty, M. Lewenstein, L. Plaja, H. C. Kapteyn, M. M. Murnane, and C. Hernández-García, "Generation of extreme-ultraviolet beams with time-varying orbital angular momentum," Science **364**, eaaw9486 (2019).
30. Y. Lin, Y. Nabekawa, and K. Midorikawa, "Generation of intense femtosecond optical vortex pulses with blazed-phase grating in chirped-pulse amplification system of Ti:sapphire laser," Appl. Phys. B **122**, 280 (2016).
31. K. Bezuhanov, A. Dreischuh, G. G. Paulus, M. G. Schatzel, and H. Walther, "Vortices in femtosecond laser fields," Opt. Lett **29**, 1942–1944 (2004).
32. Z. Guo, S. Qu, and S. Liu, "Generating optical vortex with computer-generated hologram fabricated inside glass by femtosecond laser pulses," Opt. Commun. **273**, 286–289 (2007).
33. A. Schwarz and W. Rudolph, "Dispersion-compensating beam shaper for femtosecond optical vortex beams," Opt. Lett. **33**, 2970–2972 (2008).
34. I. G. Mariyenko, J. Strohaber, and C. J. Uiterwaal, "Creation of optical vortices in femtosecond pulses," Opt. Express **13**, 7599–7608 (2005).
35. Ó. Martínez-Matos, J. A. Rodrigo, M. P. Hernández-Garay, J. G. Izquierdo, R. Weigand, M. L. Calvo, P. Cheben, P. Vaveliuk, and L. Bañares, "Generation of femtosecond paraxial beams with arbitrary spatial distribution," Opt. Lett. **35**, 652–654 (2010).
36. Y. Zhang, H. Yu, H. Zhang, X. Xu, J. Xu, and J. Wang, "Self-mode-locked Laguerre–Gaussian beam with staged topological charge by thermal-optical field coupling," Opt. Express **24**, 5514–5522 (2016).

37. N. Li, J. Huang, B. Xu, Y. Cai, J. Lu, L. Zhan, Z. Luo, H. Xu, Z. Cai, and W. Cai, "Direct generation of an ultrafast vortex beam in a CVD-graphene-based passively mode-locked Pr:LiYF$_4$ visible laser," Photon. Res. **7**, 1209–1213 (2019).
38. A. Rundquist, C. Durfee, Z. Chang, G. Taft, E. Zeek, S. Backus, M. M. Murnane, H. C. Kapteyn, I. Christov, and V. Stoev, "Ultrafast laser and amplifier sources," Appl. Phys. B **65**, 161–174 (1997).
39. W. S. Brocklesby, "Progress in high average power ultrafast lasers," Eur. Phys. J. Spec. Top. **224**, 2529–2543 (2015).
40. S. Backus, C. G. Durfee III, M. M. Murnane, and H. C. Kapteyn, "High power ultrafast lasers," Rev. Sci. Instrum. **69**, 1207–1223 (1998).
41. D. Strickl and G. Mourou, "Compression of amplified chirped optical pulses," Opt. Commun. **56**, 219–221 (1985).
42. J. Rothhardt, S. Hädrich, J. C. Delagnes, E. Cormier, and J. Limpert, "High average power near-infrared few-cycle lasers," Laser Photon. Rev. **11**, 1700043 (2017).
43. X. Chen, C. Chang, Z. Lin, P. Ding, and J. Pu, "High-energy nanosecond optical vortex output from Nd:YAG amplifiers," IEEE Photon. Technol. Lett. **28**, 1271–1274 (2016).
44. K. Yamane, Y. Toda, and R. Morita, "Ultrashort optical-vortex pulse generation in few-cycle regime," Opt. Express **20**, 18986–18993 (2012).
45. A. Berzanskis, A. Matijosius, A. Piskarskas, V. Smilgevicius, and A. Stabinis, "Conversion of topological charge of optical vortices in a parametric frequency converter," Opt. Commun. **140**, 273–276 (1997).
46. J. Qian, Y. Peng, Y. Li, P. Wang, B. Shao, Z. Liu, Y. Leng, and R. Li, "Femtosecond mid-IR optical vortex laser based on optical parametric chirped pulse amplification," Photon. Res. **8**, 421–425 (2020).
47. S. Tan, C. Zhou, A. Shirakakwa, K. Ueda, and J. Li, "Vortex Ti:sapphire laser by using an intracavity spot-defect spatial filter," Opt. Laser Technol. **96**, 76–80 (2017).
48. D. J. Kim and J. W. Kim, "Direct generation of an optical vortex beam in a single-frequency Nd:YVO$_4$ laser," Opt. Lett. **40**, 399–402 (2015).
49. J. W. Kim and W. A. Clarkson, "Selective generation of Laguerre–Gaussian (LG$_{0n}$) mode output in a diode-laser pumped Nd:YAG laser," Opt. Commun. **296**, 109–112 (2013).
50. M. Wei, W. Shiao, and Y. Lin, "Adjustable generation of bottle and hollow beams using an axicon," Opt. Commun. **248**, 7–14 (2005).
51. A. Hu, J. Lei, P. Chen, Y. Wang, and S. Li, "Numerical investigation on the generation of high-order Laguerre–Gaussian beams in end-pumped solid-state lasers by introducing loss control," Appl. Opt. **53**, 7845–7853 (2014).
52. N. Zhang, X. C. Yuan, and R. E. Burge, "Extending the detection range of optical vortices by Dammann vortex gratings," Opt. Lett. **35**, 3495–3497 (2010).
53. V. Denisenko, V. Shvedov, A. S. Desyatnikov, D. N. Neshev, W. Krolikowski, A. Volyar, M. Soskin, and Y. S. Kivshar, "Determination of topological charges of polychromatic optical vortices," Opt. Express **17**, 23374–23379 (2009).